European Polymer Journal 81 (2016) 641–649

Contents lists available at ScienceDirect

European Polymer Journal

journal homepage: www.elsevier.com/locate/europolj

Simultaneous size and density determination of polymeric colloids by continuous contrast variation in small angle X-ray scattering

Raul Garcia-Diez [a,*], Aneta Sikora [b], Christian Gollwitzer [a], Caterina Minelli [b], Michael Krumrey [a]

[a] Physikalisch-Technische Bundesanstalt (PTB), Abbestr. 2-12, 10587 Berlin, Germany
[b] Analytical Science, National Physical Laboratory, Hampton Road, TW11 0LW Teddington, UK

ARTICLE INFO

Article history:
Received 9 November 2015
Received in revised form 17 December 2015
Accepted 4 January 2016
Available online 5 January 2016

Keywords:
Polymeric particle
Colloid
SAXS
DCS
Characterization
Size
Density

ABSTRACT

Polymeric colloids are of growing importance in nanomedicine for drug or imaging agent delivery. Their characterization is a crucial task but their traceable size determination is challenging, especially for particles with a complicated inner structure. This work describes the simultaneous determination of the size distribution and the density of polymeric particles by means of continuous contrast variation in small angle X-ray scattering (SAXS), which also reveals the inner structure of the colloids. The applicability of the technique has been evaluated by the comparison with other techniques, with focus on differential centrifugal sedimentation (DCS) in terms of the measured density. A novel approach to DCS is presented, which employs two centrifuge setups to enable the density and size determination of particles with physical densities close to water.

1. Introduction

In the continuously growing world of nanotechnology, nanonoparticles have a preeminent position, employed as pharmaceutical or cosmetic products [1] and especially in the emerging field of nanomedicine. Indeed, nanoparticles open exciting new possibilities in this field as platforms for drug-delivery [2] or encapsulating imaging agents [3]. Nowadays, polymeric colloids and biodegradable nanocarriers are finding many research and medical applications [4] and are starting to undergo clinical trials [5–7].

The current advances in nanomaterial development for medical applications are focused towards tailoring polymeric nano-drug carriers with flexible surface functionalization and controlled morphologies [8,9]. Size and shape, combined with the choice of polymer and the mechanical properties, are fundamental and defining aspects of the particle functions, e.g. their *in vivo* biodistribution [10–12] or their drug-delivery efficacy [13]. Therefore, a full and consistent characterization of all properties of nanoparticles is of crucial importance and must be carefully addressed.

The characterization of polymeric nanoparticles remains a challenge due to their typically complicate internal structure [14] and requires more than a single characterization technique to detect these heterogenous compositions. For instance, electron microscopy is an effective tool for direct observation of the shape and size distribution of nanoparticles, although it cannot conclusively elucidate their internal morphology.

* Corresponding author.
E-mail address: raul.garciadiez@ptb.de (R. Garcia-Diez).

http://dx.doi.org/10.1016/j.eurpolymj.2016.01.012
0014-3057/

The use of an ensemble-average and non-destructive technique such as small-angle X-ray scattering (SAXS) arises as an appropriate alternative [15,16]. SAXS can discern differences in the radial structure of polymeric colloids and offers advantages to other methods which require prior treatment of the sample and are not averaging [17,18]. Despite being a highly informative method for the accurate characterization of polymeric particles, the difficulties in the interpretation of the scattering curves demand complementary experimental information [19].

The contrast variation method in SAXS varies systematically the electron density of the suspending medium by adding a suitable contrast agent, e.g. sucrose, in order to resolve the different contributions of the particle components to the scattering. By measuring SAXS patterns as a function of the adjusted contrast, a more detailed insight into the particle morphology can be obtained in comparison to single-contrast experiments [20]. For instance, the internal structure can be modeled in terms of the radial electron density [21–24] and the individual contribution of each polymer can be distinguished [14,25–29] as well as its density [30].

The formation of a solvent density gradient within a capillary emerges as an intelligent strategy to measure SAXS patterns at a continuous range of contrasts and, as a result, collect in a relatively short timespan an extensive data set of complementary scattering curves [31]. The continuous contrast variation technique in SAXS is ideally suited for current synchrotron radiation sources, where high brilliance and collimation permit the measurement of the scattering curves within the diffusion time of the contrast agent.

This work demonstrates the simultaneous size and density determination using this technique with 3 polymeric particles of different sizes and polymeric species. By means of an aqueous sucrose density gradient, the measurements were achieved along a large range of suspending medium densities, from water density to that of poly(methyl methacrylate)'s, highlighting the relevance of the technique across a wide spectrum of polymers.

The article discusses the applicability of this method for the traceable size determination of these colloids, where a high-resolution size distribution of the particles is presented. Focusing on a low-density colloid, different evaluation approaches to SAXS contrast variation experiments are introduced and the advantages and drawbacks of a model-free formulation like the isoscattering point position are discussed, together with the accuracy of the scattering shape factor.

In addition, a form factor model is fitted to the scattering curves to obtain decisive information about the internal morphology of the particle, which is not directly available by other techniques such as transmission scanning electron microscopy (TSEM), differential centrifugal sedimentation (DCS) [32] or atomic force microscopy (AFM).

The ability of the continuous contrast variation technique to determine the density of polymeric colloids in suspension is also discussed. Normally, the density of the suspended particles cannot be compared to the bulk density of the dry material. Such a complex question has been addressed by different methods, though with evident limitations. For example, the density of polymeric beads has been measured previously with field-flow fractionation (FFF) with high-accuracy but at the expense of *a priori* assumptions about the morphology of the particle [33–35]. Assuming the Stokes' diameter as the actual size of the colloid, recent advances in analytical ultracentrifugation allow the complementary characterization of the size, density and molecular weight of gold nanoparticles [36].

The 3 polymeric colloids were also analyzed by DCS and the results compared and discussed with those obtained by SAXS. DCS uses the sedimentation of particles through a density gradient to measure high resolution particle size distributions [37]. Its accuracy typically depends on the knowledge of the density of the particles. When the size of the particle is known, DCS can alternatively be used to measure average particle's density.

Neumann et al. [38] used two sucrose gradients resulting in different viscosities and densities, where the altered settling velocity combined with linear regression analysis was used for the calculation of the size and density of silica nanoparticles and viruses. Bell et al. [39] adopted a two gradient method based on the variation of the sucrose concentration to determine the density of the Stöber silica and the calibration standards used in DCS.

In this study, the size and density of low-density particles is independently determined by performing DCS measurements with two different discs using the sedimentation and flotation respectively of the particles through a density gradient and solving the relative Stokes' equations.

2. Materials and methods

2.1. Materials

Carboxylated polystyrene nanoparticles (PS-COOH) synthesized by multi-addition emulsion polymerization with a nominal size of 105 nm were purchased from Kisker Biotech (Steinfurt, Germany). Carboxylated poly(methyl methacrylate) colloids (PMMA-COOH) with a nominal diameter of 187 nm and plain polystyrene particles (PS-Plain) polymerized with <1 wt% of a surface-active co-monomer with a nominal diameter of 147 nm were purchased from Microparticles (Berlin, Germany). Galden® PFPE SV90 was purchased from Solvay Plastics (Brussels, Belgium).

2.2. Continuous contrast variation in SAXS

2.2.1. Density gradient preparation

Vacuum-proof borosilicate glass capillaries from Hilgenberg (Malsfeld, Germany) with a rectangular cross section of $(4.2 \pm 0.2) \times (1.25 \pm 0.05)$ mm^2, a length of (80.0 ± 0.5) mm and a wall thickness of ca. 120 μm were used for the density

gradient preparation. The suspending medium density gradient was achieved by inserting two mixtures of different densities on top of a 1 cm section of Galden with a long syringe (Sterican®G 21 × 4 3/4″, Braun, Melsungen, Germany), avoiding the contact of the needle with the capillary walls. Two dispersions of each particle with the same particle concentration were prepared: A high density mixture of the suspended colloid with a sucrose (Sigma–Aldrich, St. Louis, USA) mass fraction of 21.2%, 42.5% and 13.4% for the PS-COOH, PMMA-COOH and PS-Plain particles respectively and a dispersion of the polymeric particles diluted in ultrapure water. The bottom part of the capillary was filled with the aqueous sucrose mixture, while on the top side the diluted colloidal suspension was inserted. The concentration difference between both mixtures was less than 5%, as determined by weighing at every mixing step with a precision better than 0.1% and assuming that the diffusion of polymeric particles is at least 1000 times slower than the sucrose diffusion.

2.2.2. SAXS measurements

The scattering experiments were performed with the SAXS setup of Helmholtz-Zentrum Berlin [40] at the four-crystal monochromator beamline of PTB [41] at the synchrotron radiation facility BESSY II (Helmholtz-Zentrum Berlin, Germany). The density gradient capillary was moved in steps of 0.5 mm along the central vertical axis of the capillary, where a scattering pattern was collected for 45 to 100 s as schematically depicted in Fig. 1. At these positions, the solution transmittances were previously measured at an energy of $E = (5500.0 \pm 0.6)$ XeV in order to calibrate the suspending medium electron density [31] and at $E = (8000.0 \pm 0.8)$ eV for normalization purposes. Scattering curves with different contrasts were measured at a photon energy of 8000 eV at 3 different diffusion times, adding to a total of ca. 40 curves. The X-ray photons were collected at a distance $L = (4539 \pm 1)$ mm with a vacuum-compatible Pilatus 1 M hybrid-pixel detector (Dectris Ltd, Baden, Switzerland) with a pixel size of $d = (172.1 \pm 0.2)$ μm [42].

The rotationally symmetric scattering patterns were circularly integrated and converted to momentum transfer q using the expression $q = \frac{4\pi E}{hc} \sin\left(\frac{1}{2}\arctan\left(\frac{R}{L}\right)\right)$ where h is the Planck constant, c is the speed of light and R is the distance to the beam center. The obtained scattering curves were normalized to the exposure time, the measured suspension transmittance at 8000 eV and the incident photon flux, measured by means of a calibrated transparent silicon diode [43]. In addition, the scattering background of pure aqueous sucrose was subtracted.

2.3. Differential centrifugal sedimentation

DCS measurements were performed with a CPS DC20000 instrument (CPS Instruments, Prairieville, LA, USA) upgraded to DC24000 for the PS-Plain measurements. The radial position of the detector was measured by injecting 100 μL aliquots of water into the spinning disc initially empty until the accumulation of water produced a response in the detector. For the density gradient formation, the disc was filled with 14.4 mL of a sucrose (Amresco LLC, OH, USA) solution topped with 0.5 mL of dodecane to prevent evaporation. The detailed information of the gradients is summarized in Table 1.

The measured turbidity at a wavelength 405 nm was converted to the number of particles for each measured diameter by treating the particles as spherical Mie scatterers with no optical absorbance at the incident wavelength. Three different types of calibration particles were used: poly(vinyl chloride) colloids in water with density of 1.385 g cm^{-3} and nominal size of (223 ± 5) nm (calibrant A) and (239 ± 5) nm (calibrant B) and polybutadiene colloids in 16% sucrose mass fraction in heavy water with nominal size of (510 ± 20) nm and density of 0.91 g cm^{-3} (calibrant C). A standard disc configuration where the particles sediment through a lower density gradient was used and additionally, a more recently developed set up which makes use of a disc where colloids float through a higher density gradient was also used for PS-Plain due to their low density [44]. Measurements of PS-COOH and PMMA-COOH at 0.05% w/v concentration were performed in triplicate. PS-Plain measurements were repeated seven times for each setup. Injection volumes were 100 μL. Measurement uncertainties include both statistical and systematic uncertainty propagated from Stokes' equations.

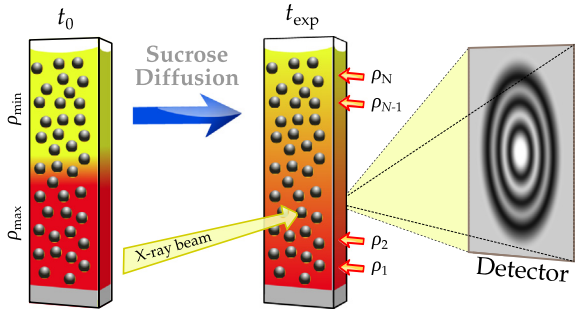

Fig. 1. Scheme of the experimental setup. At a diffusion time t_{exp}, the scattering patterns are measured with an area detector at different heights (i.e. contrasts) of the density gradient capillary.

Table 1
Parameters of the different DCS setups: composition of the sucrose gradients, average density of the gradients ρ_f, angular speed of the centrifuge Ω and type of calibrant.

	Sucrose concentration (*w/w*)	ρ_f (g cm^{-3})	Ω (rpm)	Calibrant
PS-COOH	From 2% to 8% in H_20	1.013	$2.0 \cdot 10^4$	A
PMMA-COOH	From 4% to 12% in H_20	1.025	$2.0 \cdot 10^4$	B
PS-Plain	From 2% to 8% in H_20	1.013	$2.4 \cdot 10^4$	B
PS-Plain[a]	From 4% to 12% in D_20	1.140	$2.4 \cdot 10^4$	C

[a] Low density disc.

3. Determination of the mean particle size

In Fig. 2, the SAXS curve of the PS-Plain particles in buffer at a single-contrast is shown. The large number of minima observed in the curve is remarkable and indicates the high monodispersity of the sample, which allows a traceable size determination of these colloids.

Upon trying different form factor fits detailed in the Supplementary Material, a simple core–shell structure with a sharp interface was found to be the most suitable, suggesting a heterogeneous structure which is eluded by other characterization techniques, e.g. microscopy. The obtained particle diameter was (147.0 ± 4.7) nm, where the fit uncertainty was calculated with a confidence level of one standard deviation ($k = 1$) by examining the change in χ^2 when varying the diameter. The radial electron density profile of the core–shell fit is shown in the inset of Fig. 2, where a thin shell with high density surrounds a lighter core. This structure is likely due to the non-reacted monomers in the main matrix or the highly hydrophilic behavior of the co-monomer, segregating polystyrene to the core.

The morphology was further studied using the density gradient contrast variation technique described in Section 1.2 by varying the suspending medium electron density from 333.2 to 350.2 nm^{-3}. By increasing the solvent contrast, the changes of the features in the scattering curves presented in Fig. 3 and the appearance of isoscattering points prove the multi-component composition of this colloid.

From the 40 experimental scattering curves shown in Fig. 3, a model-free size determination can be performed by locating the isoscattering points I_i, which are related to the radius R of the particle by $\tan(q^\star R) = q^\star R$ [45].

The quantification of the isoscattering points positions $q_i^\star$ was performed by calculating the relative standard deviation of each q-value across all the measured curves, as shown in the inset of Fig. 3 where the minima correspond to the fulfillment of the isoscattering condition.

The particle sizes obtained from the first 4 isoscattering points (I_1–I_4) range between 142.4 and 144.4 nm, showing a good agreement for higher q-values as well. The precision of the isoscattering point positioning decreases for increasing q as demonstrated by Kawaguchi [46] and it is exemplified by the broadening of the minima for higher q.

The data can also be analyzed by using the so-called *shape factor* or *resonant term* which can be derived from the *basic functions* approach [47,48] described in the Supplementary Material. The shape factor is defined by the scattering corresponding to the particle components impenetrable to the solvent, e.g. the external shape of the particle independently of its inner structure.

This approach is appropriate for many polymeric particles with a heterogenous morphology [20], such as the PS-Plain colloid, because it enables the size distribution determination of the particles avoiding any *a priori* consideration about the particle composition.

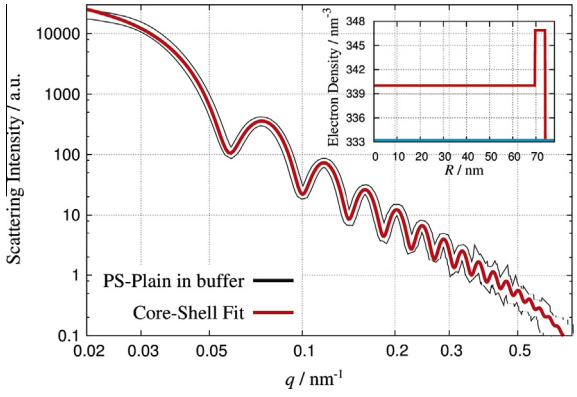

Fig. 2. Scattering curve of PS-Plain in buffer. A core–shell fit to the experimental scattering curve is presented. In the inset, the electron density radial profile of this fit is shown, assuming the core is polystyrene with a density of 339.7 nm^{-3}.

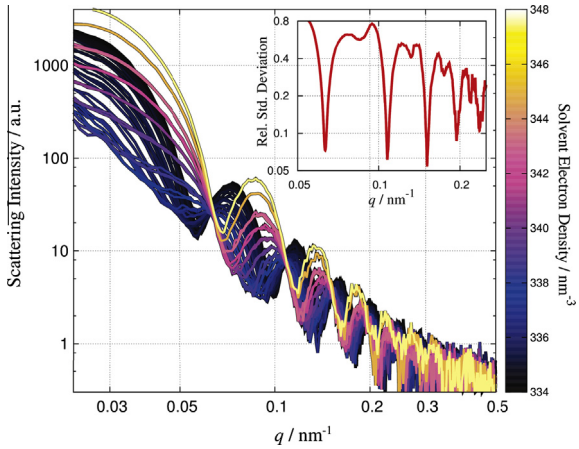

Fig. 3. SAXS curves of PS-Plain obtained by density gradient contrast variation after solvent background subtraction. The inset shows the relative standard deviation calculated from all the scattering curves, where the minima correspond to the isoscattering points I_i.

The shape factor calculated from the measured scattering curves is depicted in Fig. 4 together with the spherical model fitted to the data, which employs a simple form factor that ignores the internal structure and a gaussian size distribution. From this fit, a mean particle size of (146.8 ± 1.3) nm was determined. The fit uncertainty was determined as discussed before. By fitting an ellipsoid model to the shape factor, a sphericity of 98% was obtained.

These results highlight the applicability of this technique for the characterization of the size and shape of polymeric colloids. Additionally, the associated uncertainty calculated with this approach is 3.5 times smaller than the one obtained with the single-contrast SAXS experiment. The improvement in the size accuracy with the shape factor approach is summarized in Fig. 5, where the size of the PS-Plain particles determined by different techniques in an inter-laboratory study is also presented [49].

The figure compares the PS-Plain size measured by the ensemble techniques SAXS and DCS and the imaging methods AFM and TSEM and presents the weighted mean value of all the independent results as a gray line, which corresponds to a diameter of 145.1 nm with an associated expanded uncertainty ($k = 2$) of 1.8 nm. The SAXS results tend to larger values when modeling the scattering form factor, while the size obtained from the isoscattering points positions I_i present values slightly smaller than the calculated mean value. However, the maximum deviation from the weighted mean is less than 2%.

The DCS result is obtained by a combined analysis of two complementary centrifuge configurations as detailed in the Supplementary Material, where Fig. S1 depicts the dependency of the measured particle size on the density values for the two setups. The two setups measure the same size and density at the crossing point of the data, which occurs for a diameter of (138.8 ± 5.8) nm and a density of (1.052 ± 0.010) g cm^{-3}. The measured size fits within its uncertainty in the confidence interval of one standard deviation of the inter-laboratory comparison.

All the techniques are in very good agreement, even considering that they are based on different physical principles. The improvement in accuracy for the size determination with SAXS by using the shape factor approach is further sustained by this comparison.

This improvement was confirmed by employing the same approach for the PS-COOH colloids. The size obtained from the core–shell model fit is (99.4 ± 5.6) nm [31], while the value obtained from the shape factor calculation is (101.4 ± 2.4) nm.

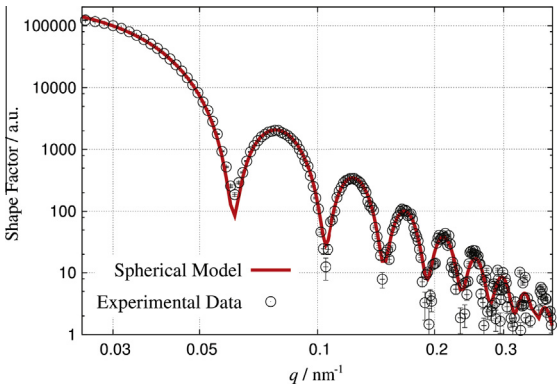

Fig. 4. Experimental shape factor of the PS-Plain colloid calculated from 40 scattering curves and the spherical form factor fitted to the data.

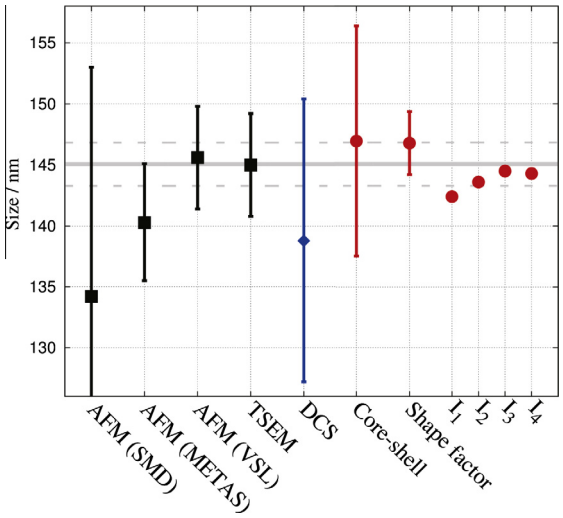

Fig. 5. Comparison of the PS-Plain average size obtained with different techniques, where the errorbars correspond to the expanded uncertainty ($k = 2$). The circles correspond to results obtained with SAXS and the diamonds to combined DCS measurements. The gray line defines the weighted mean of all the independent results. The microscopy values are obtained from Belgian Service Métrologie-Metrologische Dienst (SMD), Swiss Federal Institute of Metrology (METAS) and Dutch Metrology Institute (VSL) [49].

Again, the uncertainty associated to the size decreases by ~60%, while it is still in accordance with the size obtained with the isoscattering points positions of 101.0 nm with a standard deviation of 1.1 nm.

Due to the low polydispersity of the PMMA-COOH particles and their homogenous composition, a spherical form factor fit to the single-contrast scattering curve provides already a very accurate size (186.5 ± 2.3) nm. In this case, contrast variation experiments in SAXS show no advantages.

It has been demonstrated that the possibility to determine the particle size distribution by the scattering shape factor is a clear improvement to single-contrast SAXS techniques reducing relevantly the uncertainty, although an accurate determination of the contrast and a relatively high number of scattering curves are required.

Nevertheless, another contrast variation evaluation approach such as the isoscattering points presents as well certain assets which cannot be ignored. For instance, the independence of $q^\star$ from the sample contrast facilitates its easy application. On the other hand, the diffuseness of the isoscattering point position due to the polydispersity and ellipticity of the sample [46] arises as an indisputable drawback.

3.1. Particle polydispersity

An important attribute of polymeric colloids is their polydispersity, as the suitability for specific applications depends on their spread in size. For example, colloids are known to induce different inflammatory responses depending on their size [50]. The polydispersity degree p_d is calculated as the full width at half-maximum of the number-weighted particle size distribution divided by its average value.

The SAXS results determine a p_d for the PS-Plain colloids of 6.1%, which is an indicator of a very monodisperse distribution, as also suggested by the regular minima observed in Fig. 2. Particle polydispersities measured by DCS are also low as observed in Fig. 6, ranging from 7.8% measured with the standard set up, to 11.3% measured with the low density disc setup. The standard setup appears therefore to achieve a higher resolution size distribution. The size distribution measured by TSEM with a p_d of 8.3% shows good agreement with the ensemble techniques.

The measurements obtained by AFM provide polydispersity degrees larger than 10% [49] and, therefore, slightly broader size distributions than those calculated by SAXS, TSEM and standard DCS. This can be in part attributed to the low statistics that typically affect imaging methods, along with artefacts associated with the posterior analysis.

For instance, in the TSEM images obtained at PTB Braunschweig [49,54], smaller and larger populations with different contrasts have been observed which could affect the evaluation of the density measured by ensemble techniques in Section 3, as the particle average density might vary. Indeed, when a bimodal distribution is used to analyze the SAXS shape factor of PS-Plain particles, a second size population is found at 101 nm in agreement with TSEM, while the main mode maintains a p_d of ca. 5%.

4. Determination of the particle density

In contrast variation SAXS, the solvent electron density which matches the average electron density of the particle (ρ_0) corresponds to a minimum in the intensity of the scattering curve. In order to quantify the particle density, the scattering

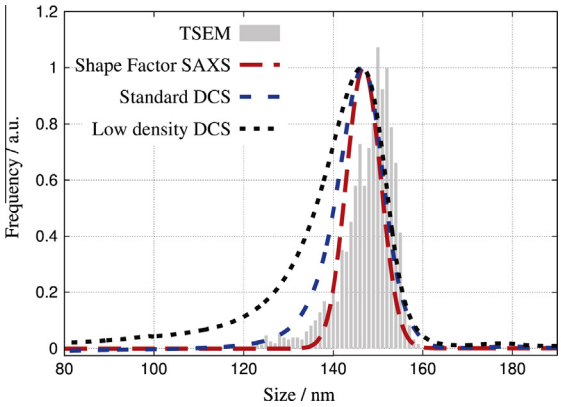

Fig. 6. Number-weighted size distribution of PS-Plain particles measured by DCS, TSEM [49] and SAXS with the scattering shape factor approach.

intensity of PS-Plain at zero angle $I(0)$ is examined along the contrast range of the experiment as shown in Fig. 7. The value of $I(0)$ was determined by extrapolation to $q \rightarrow 0$ using a spherical form factor function fitted to the available range before the first minimum.

This parameter behaves parabolically around the average electron density of the particle like $I(0) \propto (\rho_0 - \rho_{solv})^2$ [51]. From the position of the minimum, ρ_0 can thus be obtained. The parabolic fit to the data is plotted as a black line in Fig. 7 and results in $\rho_0 = (339.2 \pm 1.0)\,\mathrm{nm}^{-3}$, which is consistent with the tabulated value of dry bulk polystyrene $339.7\,\mathrm{nm}^{-3}$ [22].

The electron density is directly proportional to the physical density. Nevertheless, an assumption about the polymer (or monomer) components and their atomic structure is necessary for the calculation.Therefore, a typical value of $Z/A = 0.54$ was adopted, where Z and A are the average atomic number and mass of the polymer respectively.

In Fig. 8, the value of $(1.043 \pm 0.003)\,\mathrm{g\,cm}^{-3}$ obtained with the $I(0)$ approach from the continuous contrast variation experiment is compared to the average density of the PS-Plain colloid measured with different DCS configurations. For single disc setups, the size value used for the density calculation was 147 nm, as measured by SAXS, while combining the information from the two setups allowed the measurement of the density independently of the particle diameter, as explained in Section 2.

The results agree with each other within their stated measurement uncertainties, although DCS measurements exhibit slightly higher densities than SAXS. Typical causes of systematic errors in DCS are the inaccuracy of the size and density of the calibration standard and the thermal variation in the centrifuge gradient during the measurements, which affect its viscosity and density [52]. A temperature variation within the gradient of about 7 °C before and after measurements was detected and a period of 30 min was considered appropriate to reach reliable thermal equilibrium. In the low density disc configuration, the accuracy of the average density of the D_20 sucrose gradient becomes an important source of uncertainty.

In SAXS, the uncertainty is associated to the vertical size of the focused X-ray beam [31]. Furthermore, the result can be affected by the polymeric composition of the colloid, and therefore, the assumption of Z/A.

The applicability of the continuous contrast variation techniques is further discussed by comparing with DCS for higher-density polymeric colloids, as summarized in Fig. 8. The density of the PS-COOH particles derived from the $I(0)$ approach is in excellent agreement with that measured by DCS using a standard configuration and assuming a particle diameter of

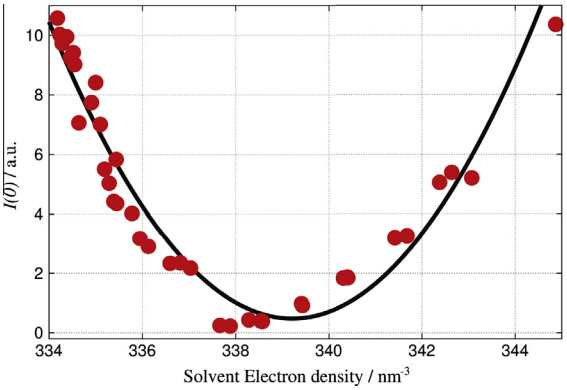

Fig. 7. Intensity at zero-angle of PS-Plain particles as a function of the solvent electron density measured with continuous contrast variation in SAXS. The minimum defines the average electron density of the particle.

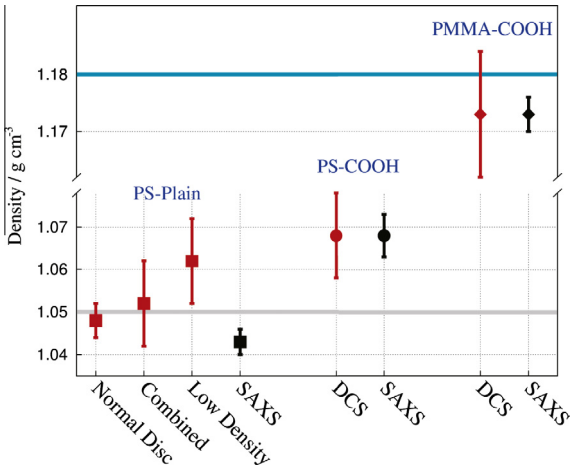

Fig. 8. Comparison between the physical densities of 3 polymeric colloids measured with SAXS using the $I(0)$ approach and DCS: PS-Plain (squares), PS-COOH (circles) and PMMA-COOH (diamonds). The nominal densities of polystyrene (1.05 g cm^{-3}) and PMMA (1.18 g cm^{-3}) are also shown in the plot as horizontal lines [22].

99.4 nm, which was obtained by SAXS. These core–shell particles, more dense than polystyrene [31], illustrate the tendency during the emulsion polymerization to segregate polar and nonpolar components [29].

Similarly, the density of the PMMA-COOH colloids was measured using the standard DCS setup and assuming a diameter of 186.5 nm, as measured by SAXS. This value is compared to the density obtained by computing the intensity at zero-angle of a continuous contrast variation experiment. Again, both techniques are in excellent agreement and reveal a physical density slightly lower than the expected PMMA density of 1.18 g cm^{-3} [22].

This result highlights the fact that the density of polymeric colloids in suspension may vary from that of bulk materials, for example dry particles. For instance, a volume variation can be expected when going from the MMA monomer to the polymer PMMA [53] which might reduce the colloid density.

5. Conclusions

This work demonstrates how continuous contrast variation in SAXS emerges as a powerful characterization technique for polymeric colloids, which can determine their size and density in a traceable way. For instance, the accuracy in the density information achieved with the density gradient technique is remarkable and extends along a rather large density range of polymers.

Since contrast variation in SAXS is very sensitive to small electron density differences in the colloid morphology, the applicability of this method to investigate the inner structure of 3 different particles has been discussed. This is of paramount importance in polymeric particle characterization because the direct observation by imaging techniques is inadequate for this purpose.

The detection of core–shell structures in polymeric colloids appears as essential for understanding the possible processes occurring during the particle formation, e.g. the consequences of emulsion polymerization synthesis.

These results were compared successfully with other techniques. In particular, SAXS measurements of the density of these colloids are in excellent agreement with those performed by DCS. The use of a novel DCS setup is also shown, which makes use of a centrifuge disc where the colloids float through a gradient of higher density, in contrast to a standard setup where the particles typically sediment. The use of the two complementary DCS configurations allowed the simultaneous determination of both the size and density of polymeric colloids consistently with the SAXS results.

Furthermore, different evaluation approaches to contrast variation SAXS data are examined in detail. The isoscattering point framework is found to be of easy utilization and very appropriate for spherical and quite monodisperse colloids. On the other hand, the calculation of the scattering shape factor arises as a precise sizing technique which can additionally provide an insight into the particle shape, although a high number of measurements with different contrasts and an accurate calibration of the system are required.

With the continuous contrast variation technique in SAXS, a more precise characterization of the morphology of polymeric particles is achieved which opens new opportunities to investigate complex polymeric colloids. Besides, both ensemble techniques presented in this paper arise as powerful methods which can describe simultaneously the density and size distribution of polymeric colloids at the nanoscale.

Acknowledgements

The authors are grateful to Dr. A. Hoell of the Helmholtz-Zentrum Berlin for the research cooperation with the HZB SAXS instrument and to L. Cibik and S. Langner of PTB for their technical support. This work was funded by the European Metrol-

ogy Research Programme (EMRP) and by the UK Innovation Research & Development programme. The EMRP is jointly funded by the EMRP participating countries within EURAMET and the European Union.

Appendix A. Supplementary material

DCS evaluation and Stokes' equations, scattering form factor, shape factor and contrast variation. Supplementary data associated with this article can be found, in the online version, at http://dx.doi.org/10.1016/j.eurpolymj.2016.01.012.

References

[1] S.S. Guterres, M.P. Alves, A.R. Pohlmann, Drug Target Insights 2 (2007) 147–157.
[2] A.Z. Wang, R. Langer, O.C. Farokhzad, Ann. Rev. Med. 63 (2012) 185–198, http://dx.doi.org/10.1146/annurev-med-040210-162544.
[3] L. Tao, W. Hu, Y. Liu, G. Huang, B.D. Sumer, J. Gao, Exp. Biol. Med. 236 (2011) 20–29, http://dx.doi.org/10.1258/ebm.2010.010243.
[4] M.J. Vicent, R. Duncan, Trends Biotechnol. 24 (2006) 39–47, http://dx.doi.org/10.1016/j.tibtech.2005.11.006.
[5] T. Patel, J. Zhou, J.M. Piepmeier, W.M. Saltzman, Adv. Drug Deliv. Rev. 64 (2012) 701–705, http://dx.doi.org/10.1016/j.addr.2011.12.006.
[6] M. Beija, R. Salvayre, N. Lauth-de Viguerie, J.-D. Marty, Trends Biotechnol. 30 (2012) 485–496, http://dx.doi.org/10.1016/j.tibtech.2012.04.008.
[7] H. Cabral, K. Kataoka, J. Control Release 190 (2014) 465–476, http://dx.doi.org/10.1016/j.jconrel.2014.06.042.
[8] L.E. Euliss, J.A. DuPont, S. Gratton, J. DeSimone, Chem. Soc. Rev. 35 (2006) 1095, http://dx.doi.org/10.1039/b600913c.
[9] Z. Yang, W.T.S. Huck, S.M. Clarke, A.R. Tajbakhsh, E.M. Terentjev, Nat. Mater. 4 (2005) 486–490, http://dx.doi.org/10.1038/nmat1389.
[10] M. Vittaz, D. Bazile, G. Spenlehauer, T. Verrecchia, M. Veillard, F. Puisieux, D. Labarre, Biomaterials 17 (1996) 1575–1581, http://dx.doi.org/10.1016/0142-9612(95)00322-3.
[11] S. Mitragotri, J. Lahann, Nat. Mater 8 (2009) 15–23, http://dx.doi.org/10.1038/nmat2344.
[12] N. Doshi, S. Mitragotri, Adv. Funct. Mater. 19 (2009) 3843–3854, http://dx.doi.org/10.1002/adfm.200901538.
[13] K.W. Powers, S.C. Brown, V.B. Krishna, S.C. Wasdo, B.M. Moudgil, S.M. Roberts, Toxicol. Sci. 90 (2006) 296–303, http://dx.doi.org/10.1093/toxsci/kfj099.
[14] D. Beyer, W. Lebek, W.-D. Hergeth, K. Schmutzler, Colloid. Polym. Sci 268 (1990) 744–748, http://dx.doi.org/10.1007/BF01411105.
[15] B.R. Leonard Jr, J.W. Anderegg, P. Kaesberg, W.W. Beeman, J. Appl. Phys. 23 (1952) 152.
[16] F. Motzkus, Acta Crystall. 12 (1959) 773–786, http://dx.doi.org/10.1107/S0365110X59002250.
[17] M.S. Silverstein, Y. Talmon, M. Narkis, Polymer 30 (1989) 416–424, http://dx.doi.org/10.1016/0032-3861(89)90006-2.
[18] J.E.L. Joensson, H. Hassander, L.H. Jansson, B. Toernell, Macromolecules 24 (1991) 126–131, http://dx.doi.org/10.1021/ma00001a021.
[19] O.O. Mykhaylyk, in: Proceedings of the International Conference Nanomaterials: Applications and Properties, Sumy State University Publishing, 2012, p. 01PCN04.
[20] J. Bolze, M. Ballauff, T. Rische, D. Rudhardt, J. Meixner, Macromol. Chem. Phys. 205 (2004) 165–172, http://dx.doi.org/10.1002/macp.200300117.
[21] N. Dingenouts, Y.-S. Kim, M. Ballauff, Macromol. Rapid Commun. 15 (1994) 613–617, http://dx.doi.org/10.1002/marc.1994.030150707.
[22] N. Dingenouts, J. Bolze, D. Pötschke, M. Ballauff, in: A. Abe (Ed.), Polymer Latexes – Epoxide Resins – Polyampholytes, Advances in Polymer Science, Springer-Verlag, Berlin-Heidelberg, 1999, pp. 1–47.
[23] M. Ballauff, Adv. Eng. Mater. 13 (2011) 793–802, http://dx.doi.org/10.1002/adem.201000303.
[24] M. Ballauff, J. Bolze, N. Dingenouts, P. Hickl, D. Pötschke, Macromol. Chem. Phys. 197 (1996) 3043–3066, http://dx.doi.org/10.1002/macp.1996.021971001.
[25] R. Grunder, Y.S. Kim, M. Ballauff, D. Kranz, H.-G. Müller, Angew. Chem. Int. Ed. 30 (1991) 1650–1652, http://dx.doi.org/10.1002/anie.199116501.
[26] R. Grunder, G. Urban, M. Ballauff, Colloid. Polym. Sci. 271 (1993) 563–572, http://dx.doi.org/10.1007/BF00657987.
[27] R.H. Ottewill, S.J. Cole, J.A. Waters, Macromol. Symp. 92 (1995) 97–107, http://dx.doi.org/10.1002/masy.19950920110.
[28] J. Bolze, K.D. Hörner, M. Ballauff, Langmuir 13 (1997) 2960–2964, http://dx.doi.org/10.1021/la970106g.
[29] N. Dingenouts, T. Pulina, M. Ballauff, Macromolecules 27 (1994) 6133–6136, http://dx.doi.org/10.1021/ma00099a030.
[30] O.O. Mykhaylyk, A.J. Ryan, N. Tzokova, N. Williams, J. Appl. Crystall. 40 (2007) s506–s511, http://dx.doi.org/10.1107/S0021889807001616.
[31] R. Garcia-Diez, C. Gollwitzer, M. Krumrey, J. Appl. Crystall. 48 (2015) 20–28, http://dx.doi.org/10.1107/S1600576714024455.
[32] L.A. Fielding, O.O. Mykhaylyk, S.P. Armes, P.W. Fowler, V. Mittal, S. Fitzpatrick, Langmuir 28 (2012) 2536–2544, http://dx.doi.org/10.1021/la204841n.
[33] J.C. Giddings, G. Karaiskakis, K.D. Caldwell, Sep. Sci. Technol. 16 (1981).
[34] F.-S. Yang, K.D. Caldwell, J.C. Giddings, J. Colloid. Interf. Sci. 92 (1983) 81–91, http://dx.doi.org/10.1016/0021-9797(83)90118-2.
[35] K.D. Caldwell, H.K. Jones, J.C. Giddings, Colloid. Surf. 18 (1986) 123–131, http://dx.doi.org/10.1016/0166-6622(86)80199-8.
[36] R.P. Carney, J.Y. Kim, H. Qian, R. Jin, H. Mehenni, F. Stellacci, O.M. Bakr, Nat. Commun. 2 (2011) 335, http://dx.doi.org/10.1038/ncomms1338.
[37] C. Minelli, R. Garcia-Diez, A.E. Sikora, C. Gollwitzer, M. Krumrey, A.G. Shard, Surf. Interf. Anal. 46 (2014) 663–667, http://dx.doi.org/10.1002/sia.5381.
[38] A. Neumann, W. Hoyer, M.W. Wolff, U. Reichl, A. Pfitzner, B. Roth, Colloid. Surf. B 104 (2013) 27–31, http://dx.doi.org/10.1016/j.colsurfb.2012.11.014.
[39] N.C. Bell, C. Minelli, J. Tompkins, M.M. Stevens, A.G. Shard, Langmuir 28 (2012) 10860–10872, http://dx.doi.org/10.1021/la301351k.
[40] G. Gleber, L. Cibik, S. Haas, A. Hoell, P. Müller, M. Krumrey, J. Phys. Conf. Ser. 247 (2010) 012027, http://dx.doi.org/10.1088/1742-6596/247/1/012027.
[41] M. Krumrey, G. Ulm, Nucl. Instrum. Meth. A 467–468 (2001) 1175–1178, http://dx.doi.org/10.1016/S0168-9002(01)00598-8.
[42] J. Wernecke, C. Gollwitzer, P. Müller, M. Krumrey, J. Synchrotron. Rad. 21 (2014) 529–536, http://dx.doi.org/10.1107/S160057751400294X.
[43] M. Krumrey, G. Gleber, F. Scholze, J. Wernecke, Measur. Sci. Technol. 22 (2011) 094032, http://dx.doi.org/10.1088/0957-0233/22/9/094032.
[44] S. Fitzpatrick, Structure and Method for Centrifugal Sedimentation Particle Size Analysis of Particles of Lower Density Than Their Suspension Medium, US Patent 5786898 A, 1998.
[45] T. Kawaguchi, T. Hamanaka, T. Mitsui, J. Colloid. Interf. Sci. 96 (1983) 437–453, http://dx.doi.org/10.1016/0021-9797(83)90046-2.
[46] T. Kawaguchi, T. Hamanaka, J. Appl. Crystall. 25 (1992) 778–784, http://dx.doi.org/10.1107/S0021889892006368.
[47] H.B. Stuhrmann, R.G. Kirste, Z. Phys. Chem. 46 (1965) 247–250, http://dx.doi.org/10.1524/zpch.1965.46.34.247.
[48] H.B. Stuhrmann, R.G. Kirste, Z. Phys. Chem. 56 (1967) 334–337, http://dx.doi.org/10.1524/zpch.1967.56.56.334.
[49] A. Nicolet, F. Meli, E. Van der Pol, Y. Yuana, C. Gollwitzer, M. Krumrey, P. Cizmar, E. Buhr, J. Petry, N. Sebaihi, B. de Boeck, V. Fokkema, R. Bergmans, R. Nieuwland, Measur. Sci. Technol. (2016).
[50] T. Kusaka, M. Nakayama, K. Nakamura, M. Ishimiya, E. Furusawa, K. Ogasawara, PLoS ONE 9 (2014) e92634, http://dx.doi.org/10.1371/journal.pone.0092634.
[51] M.V. Avdeev, J. Appl. Crystall. 40 (2007) 56–70, http://dx.doi.org/10.1107/S0021889806049491.
[52] M. Kamiti, D. Boldridge, L.M. Ndoping, E.E. Remsen, Anal. Chem. 84 (2012) 10526–10530, http://dx.doi.org/10.1021/ac3022086.
[53] F.S. Nichols, R.G. Flowers, Ind. Eng. Chem. 42 (1950) 292–295, http://dx.doi.org/10.1021/ie50482a024.
[54] T. Klein, E. Buhr, K.-P. Johnsen, C.G. Frase, Measur. Sci. Technol. 22 (2011) 094002.